Journal of Mechanical Engineering and Sciences
ISSN (Print): 2289-4659; e-ISSN: 2231-8380
Volume 13, Issue 3, pp. 5703-5716, September 2019

DOI: https://doi.org/10.15282/jmes.13.3.2019.30.0456

Modeling and experimental validation of the vibration in an unbalance multi-stage rotor

W. Cruz [1], N. Arzola [2], O. Araque [3*]

[1] Universidad Nacional de Colombia, Sede Bogotá, Facultad de Ingeniería, Departamento de Ingeniería Mecánica y Mecatrónica, Grupo de Investigación en Diseño Óptimo Multidisciplinario, Cra. 30 no. 45-03, Bogotá, 11132, Colombia.
[2] Universidad Nacional de Colombia, Sede Bogotá, Facultad de Ingeniería, Departamento de Ingeniería Mecánica y Mecatrónica, Grupo de Investigación en Diseño Óptimo Multidisciplinario, Cra. 30 no. 45-03, Bogotá, 111321, Colombia, narzola@unal.edu.co
[3*] Department of Mechanical Engineering, Universidad de Ibagué, Ibagué 730001, Colombia,
*Email: oscar.araque@unibague.edu.co

ABSTRACT

This work proposes a finite element method model to predict lateral vibration phenomena arising in the multi-stage rotor (seven stages) with unbalance, including damping and gyroscopic effects. The rotor dynamic analysis includes mathematical and experimental determination of the first and second critical speeds of the rotor and the assessment of the effects induced by the different unbalance combinations. When the rotor is balanced, the first critical speed is presented at 48 Hz (2880 rpm). The results show that while considering the unbalance effects in the impellers, critical speeds move to lower frequencies adding an unbalance mass of 2 g in any of the impellers, this speed is presented at 25 Hz (1500.1 rpm). Finally, the results obtained analytically achieved a good degree of correspondence presents a percentage variation of up to 8.7% with experimental validation tests.

***Keywords**:* Rotor dynamics; critical speed; lateral vibration; finite element analysis; stiffness; damping.

INTRODUCTION

The development and study of rotor dynamics began in 1869, when Rankine crafted the concept of critical speed [1]. The development continues today with increasingly complex studies owing to the need to study machines with slender rotational elements at high operating speeds.

Rankine, Stodola, Jeffcott, Linn, Goodman, Lund and Childson are some of the authors that prompted new research in the field of rotor dynamics. The Jeffcott rotor model is undoubtedly the most important model in the analysis of rotors since, as described by Rieger [1], Jeffcott demonstrated that rotary systems have more than one critical speed using this model, contrary to Rankine who assumed that the equipment only had one critical speed: their operation limit. On his part, Reyes [2] performed the harmonic analysis of a rotor composed of two disks mounted on a shaft and flexible supports, concluding that, in rotors

with symmetrical flexible supports, natural frequencies are in pairs. This researcher found that when the gyroscopic effect is added, natural paired frequencies are separated as the angular speed increases. Yao and others [3] describe the identification and optimization of unbalance parameters in rotor-bearing systems. Two methods are proposed for the identification of the unbalance characteristics: the first is based on modal expansion combined with the use of optimization algorithms, and the second relates to the use of modal expansion technique applied to the inverse problem concluded that identification and optimization procedure for the integrated modal expansion/inverse problem approach provides more accurate predictions than the ones given by the pure modal expansion method. Genta [4] determined that any damping inherent in the material of a multi-stage rotor with multiple supports does not affect the response to its unbalance if the bearings are isotropic. However, the converse occurs when the bearings are orthotropic, which generates elliptical synchronous orbits. Unbalance is defined as an uneven distribution of mass causing the mass axis to differ from the bearing axis.

Currently, several authors have developed models that use a finite element commercial programs as an interface to simulate and determine the dynamic characteristics of rotors. The models established for the rotors under study are based on the interaction of the fundamental components: shaft, disks, bearings and unbalanced masses [5, 6, 7]. On the research [8] numerical analysis to calculate relative natural frequencies was using genetic algorithms approach. Has been found to be quite reliable for fault diagnosis by monitoring the possible variations in the relative natural frequencies of a free-free beam element

The research studies conducted have mostly used software tools based on the finite element method (FEM), to achieve reliable and accurate results on the dynamic behavior of the rotors.

At the industrial level, it is common to use quick mathematical methods the research [9], proposed to calculate maximum axis radio of the unbalance response orbit for a geared rotor system. In his research the proposed method is validated through three applications, a spur geared two-shaft rotor system, a spur geared multi-shaft rotor system and a helical geared multi-shaft rotor system. A classical modal synthesis is also employed as a comparison. Results show that proposed analytical solutions are consistent with the numerical results and have advantages over the modal synthesis.

The objective of this work is to propose a FEM model for predicting the lateral vibration phenomenon that occurs in a multi-stage rotor with unbalance that considers damping and gyroscopic effects. Concurrently, the results obtained by FEM were validated with measurements made in an experimental rotor dynamics facility.

MATERIALS AND METHODS

In this section, the procedures and tools, both theoretical and experimental are used to conduct this research. The geometrical and inertial characteristics of the rotor and its impellers are defined along the elastic and damping properties of the rotor and its supports. The numerical model is developed through the FEM.

Numerical Model

The general equation that governs the behavior of the rotor can be written as follows:

$$[M]\{\ddot{x}\} + [C]\{\dot{x}\} + [K]\{x\} = \{F_{(t)}\} \quad (1)$$

where, [M] is the mass matrix, [C] is the damping matrix, [K] is the stiffness matrix, and {F} is the external force vector. Besides$\{\ddot{x}\}$,$\{\dot{x}\}$ and $\{x\}$ are the acceleration, speed, and position vectors, respectively.

Considering the properties of the supports in the rotor model, the global matrices are described as follows:

$$[M_f] = [M_r] + [M_c^e] \quad (2)$$

$$[C_f] = [C_r] + [C_d] + [C_c] \quad (3)$$

$$[K_f] = [K_r] + [K_c^e] \quad (4)$$

where $[M_c^e]$ and $[K_c^e]$ are elements of mass and stiffness, respectively, $[M_r]$ is the mass matrix of the disk, $[C_r]$ is the support damping matrix, $[K_r]$ is the support stiffness matrix, $[C_d]$ is the gyroscopic effects matrix of the disk, and $[C_C]$ is the gyroscopic effects matrix of the shaft.

The main boundary conditions for the system are defined for the supports. The bearings are considered flexible and with damping features, these characteristics are established in the nodes of the rotor elements located in the position of the journal bearing.

The stiffness matrix of the supports is expressed as:

$$[K_r] = \begin{bmatrix} k_{xx} & k_{xy} & 0 & 0 \\ k_{yx} & k_{yy} & 0 & 0 \\ 0 & 0 & 0 & 0 \\ 0 & 0 & 0 & 0 \end{bmatrix} \quad (5)$$

While, the damping matrix of the supports is expressed as:

$$[C_r] = \begin{bmatrix} C_{xx} & C_{xy} & 0 & 0 \\ C_{yx} & C_{yy} & 0 & 0 \\ 0 & 0 & 0 & 0 \\ 0 & 0 & 0 & 0 \end{bmatrix} \quad (6)$$

These last two matrices (Equations 5 and 6) increase the sensitivity of the dynamic behavior of the rotor, since they enable the possibility of movement of the supports.

If the rotor motion Equation (1) is represented through state vectors, where $\dot{y} = [\ddot{x}, \dot{x}]$ and $y = [x', x]$, the equation is as follows [10]:

$$\begin{bmatrix} -K & 0 \\ 0 & M \end{bmatrix} \dot{y} + \begin{bmatrix} 0 & K \\ K & C \end{bmatrix} y = 0 \quad (7a)$$

$$\begin{bmatrix} -l & 0 \\ 0 & M \end{bmatrix} \dot{y} + \begin{bmatrix} 0 & l \\ K & C \end{bmatrix} y = 0 \quad (7b)$$

where, *0* is the null matrix. Assuming that the first matrix is -*S* and the second −*R*, the following expression can be established:

$$-S\dot{y} + R_y = 0 \quad (8)$$

Now, assuming a solution like $y = CYe^{\lambda t}$, an eigen-problem is generated so that (6) can be rewritten as follows:

$$[R - \lambda S]Y = 0 \quad (9a)$$

$$[A - \lambda S]Y = 0 \quad (9b)$$

$$\left[R^{-1}S - \frac{1}{\lambda}l\right]Y = 0 \quad (9c)$$

Knowing that $A = R^{-1}S$, eigenvalues λ can be extracted from matrix A through Ansys and Matlab.

Rotor Geometry

Figure 1 shows the geometry of the seven-stage rotor on which the present research is conducted.

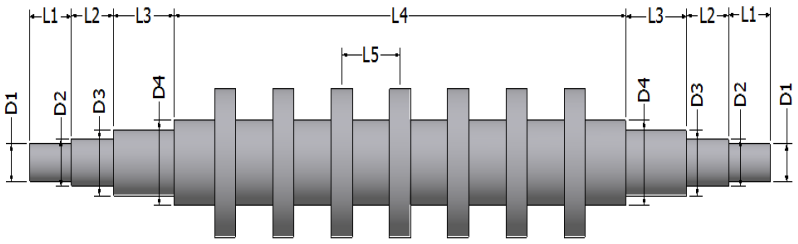

Figure 1. Geometry of the seven-stage rotor developed in CAD.

The rotor dynamic system studied comprises a rotor with seven rigid disks supported by two bearings. Disks and shaft are made with stainless steel with Young's modulus of 193 GPa, Poisson's ratio is 0.3 and density of 8080 kg/m^3. Table 1 shows the main parameters and geometrical features of the rotor.

Table 1. Main parameters and geometry of the seven-stage rotor.

Subject	Specification
Length L1	38.0 mm
Length L2	38.0 mm
Length L3	55.0 mm
Length L4	410.0 mm
Length L5	52.8 mm
Diameter D1	25.4 mm
Diameter D2	31.75 mm
Diameter D3	38.1 mm
Diameter D4	57.15 mm
Impeller external diameter	93.0 mm
Impeller Internal diameter	57.15 mm
Impeller Thickness	19.0 mm
Shaft and impellers material	Stainless steel 304
Dynamic viscosity of the oil	2.87 e-5 Pa s
Minimum oil film thickness	0.0091 mm

Rotor FEM Model

The modeling of the lateral vibration phenomenon was conducted in Matlab geared toward the solution of the mathematical formulation. For the analysis, the rotor was divided into 28 elements to have a simplify discretization but a good accuracy level in the results of the mathematical model. In Figure 2 the discretization of the multistage-rotor is shows.

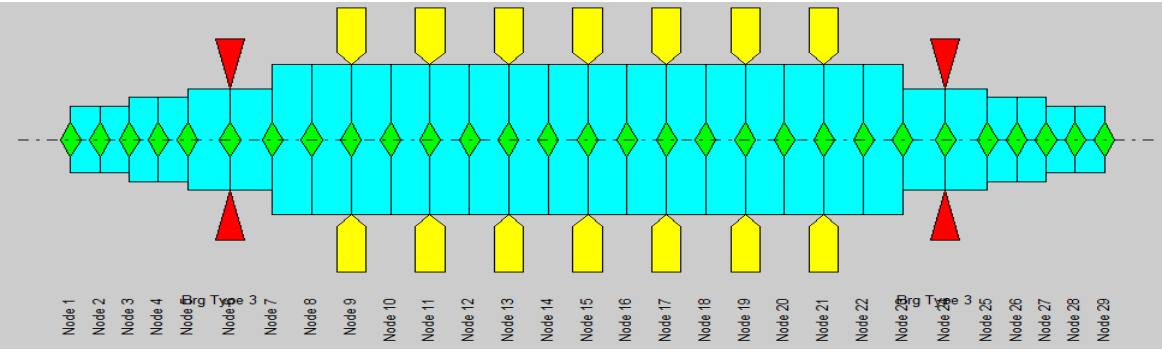

Figure 2. Discretization of the multi-stage rotor in 28 elements.

The seven impellers are located at nodes 9, 11, 13, 15, 17, 19, and 21, respectively, while the bearings are located at nodes 6 and 24.

When subjected to vibrations, the film of oil contained in the journal bearings adds support and damping to the rotor. The stiffness and damping coefficients are calculated according to the type of bearing, diameter, viscosity, load, speed, radial clearance and Sommerfeld number [11]. According to Figure 3 for journal bearings representation, the Table 2 presents the stiffness and damping properties of the journal bearings.

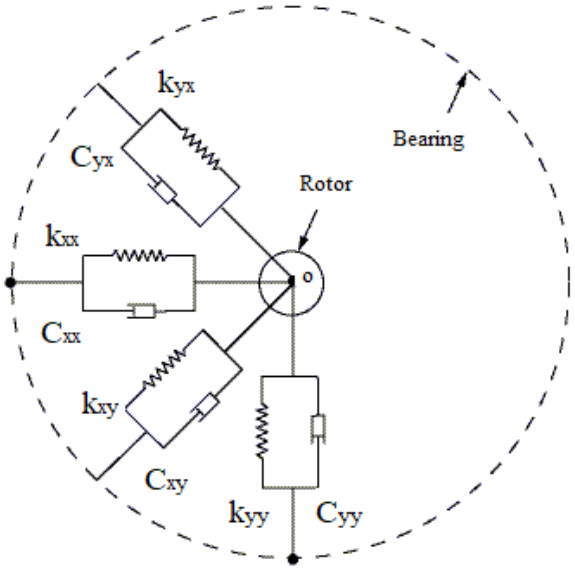

Figure 3. Diagram of the location of stiffness and damping properties for the journal bearings.

Table 2. Bearings stiffness and damping properties.

Stiffness (N/m)	Damping (Ns/m)
$k_{yy} = 3.19 \times 10^5$	$C_{yy} = 181.5$
$k_{xx} = 1.78 \times 10^6$	$C_{xx} = 1493.4$
$k_{yx} = 1.38 \times 10^5$	$C_{yx} = 346.3$
$k_{xy} = 9.76 \times 10^5$	$C_{xy} = 1493.4$

The multi-stage rotor was modeled through the Ansys commercial software for finite elements using 3D elements. First, a mesh convergence study was carried out in order to find a proper finite element size. This study allowed an accurate solution and not overly demanding of CPU time. The results obtained through Ansys will be used as an additional theoretical way of checking the current theoretical model implemented in Matlab. Figure 4 shows the model generated in Ansys with a mesh that has 259 766 nodes and 147 169 elements respectively.

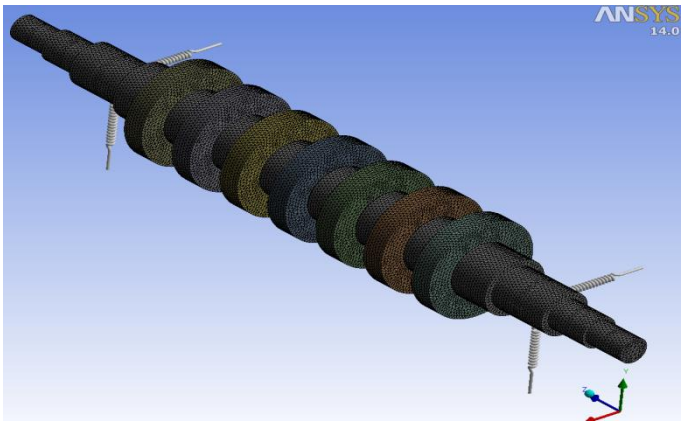

Figure 4. Ansys model of the seven-stage rotor.

The Solid187 element was used to model the rotor because, apart from being appropriate for modeling irregular meshes produced with *CAD* software, it also considers movement behavior as a quadratic interpolation function.

The bearings are modeled with *Combin14* elements that are uniaxial tension-compression elements with up to three degrees of freedom in each node and consider the effect of stiffness and damping. The *CONTA174* and *Targe170* elements are used to interconnect the different parts of the rotor. The coefficients of stiffness and damping in the lateral directions are introduced as real constants, and the gyroscopic effects on the rotor are activated by the *CORIOLIS* command.

Experimental Design

In order to validate the current theoretical model of the rotor an experimental study was conducted. Through tests, this study helped to obtain the natural critical frequencies where

the vibration phenomenon is presented in the seven-stage rotor; thus, these results contrast with the results obtained using the solution of the numerical model.

The experimental installation is composed of six main systems (structural support, power source, data acquisition system, security system, rotating system and control system) and each of them groups together components with specific functions for their proper operation. The seven-stage rotor used for experimentation is shown in Figure 5.

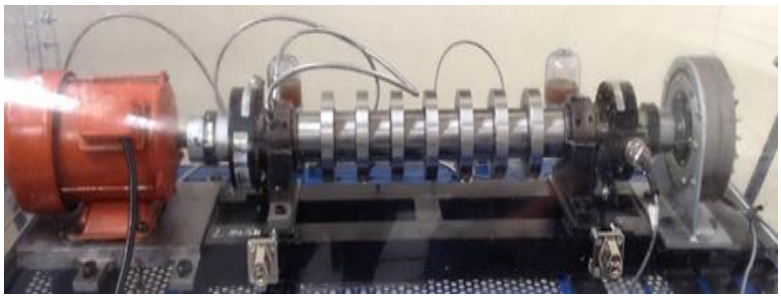

Figure 5. Seven-stage rotor used for experimentation.

The dynamic behavior of the rotor is analyzed through the evaluation of levels of lateral vibration severity in the spectrum graphs, rotor performance analysis when passing through critical speeds and orbit graphs. The lateral vibration of the rotor is registered with two accelerometers installed orthogonally in the journal bearings, according to technical standard ISO 10816 [12]. The signals of the accelerometers are taken to a computer and using the code developed in the NI Signal Express software [13]; the fundamental wave-time, spectrum and orbit graphics are displayed.

In order to determine the dynamic behavior of the rotor with unbalance, test unbalance masses of 2 grams were placed in the impellers. After registering the corresponding graphs, the unbalance mass is changed to another angular position. This procedure was performed for each impeller. The seven impellers use dovetail housing to facilitate the addition of unbalance masses (see details in Figure 6).

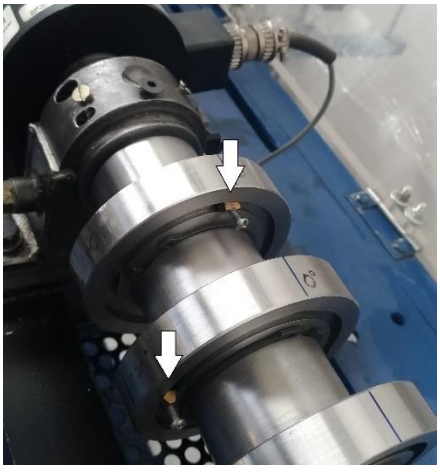

Figure 6. Detail showing dovetail machining where the unbalance masses are installed.

RESULTS AND DISCUSSION

Experimental tests were conducted, and it was observed that the highest instability of the rotor occurs at a frequency range between 46 Hz and 50 Hz; mainly at a frequency of 48 Hz, where the first lateral critical speed is observed.

The wave-time graph at 48 Hz, as seen in the Figure 7 and Figure 8 respectively, shows an increase in its amplitude with respect to that observed for previous frequencies. Similarly, the wave maintains a non-constant behavior in both the positive and the negative regions.

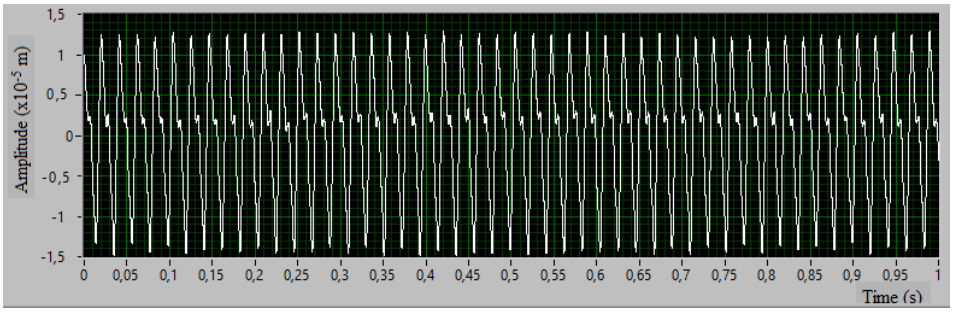

Figure 7. Wave amplitude vs time at 48 Hz for the horizontal axis.

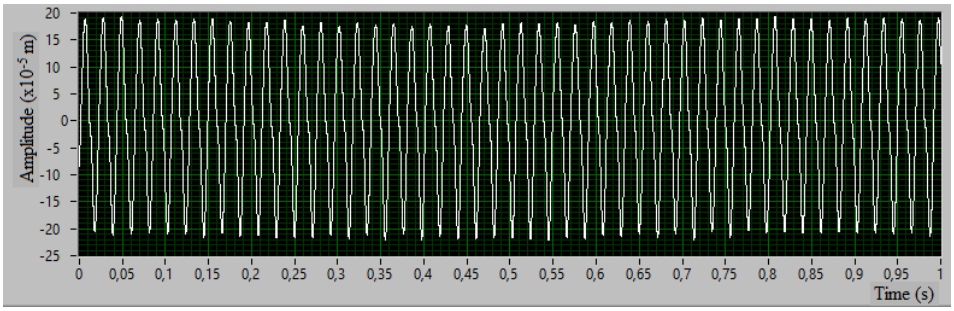

Figure 8. Wave amplitude vs time at 48 Hz for the vertical axis.

At spectral analysis level, as seen in the Figure 9 and Figure 10 respectively, there is evidence of an increase of ~1.4 times in the vibration severity levels in the bearing owing to the rotor passing through a zone of critical speed. In the domain of frequency, it is possible to appreciate how the frequency 1x is the one with the greatest amplitude. The predominance of frequencies peaks at 1x, 2x, 3x, etc. is a characteristic of the phenomenon of lateral vibration for a rotor operating close to the critical speed.

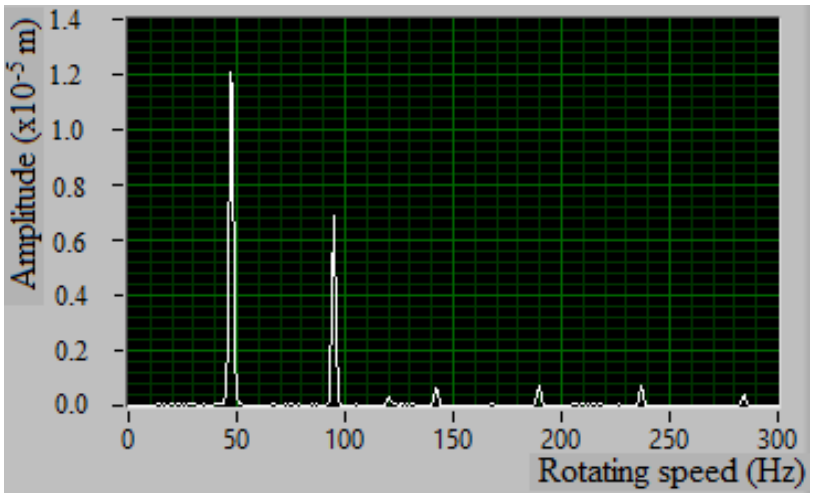

Figure 9. Diagram of the vibration amplitude vs the rotating speed for the horizontal axis.

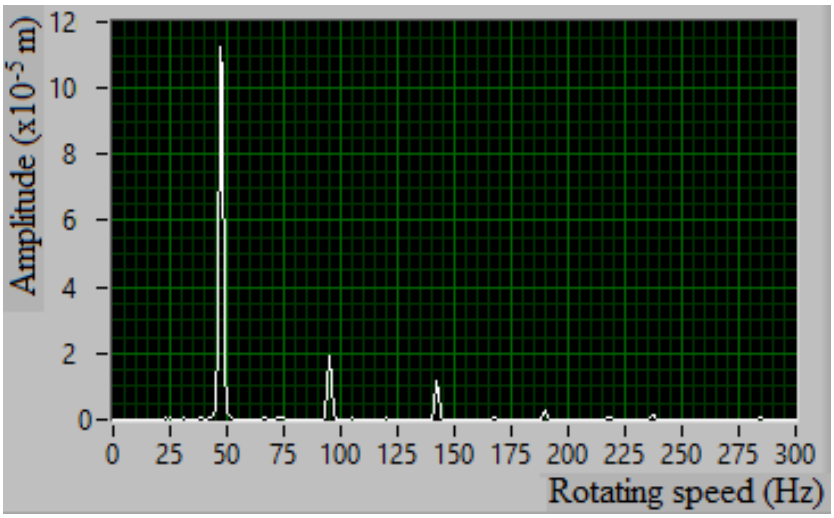

Figure 10. Diagram of the vibration amplitude vs the rotating speed for the vertical axis.

The bearing evidences a predominance of 1x frequency, which is characteristic of the lateral vibration phenomenon caused by the critical speed.

According to Figure 11, the orbit of the rotor at 48 Hz (critical rotating speed) evidences an overlap of vibration amplitude signals much higher than the behavior found at lower or higher frequencies. An internal loop is observed in the axis rotation direction, a common occurrence when the rotor passes through a critical speed region. The rotary behavior of the rotor at 48 Hz is presented by the orbit diagram which maintains a ratio of 17:1, indicating the abnormal operation of the rotor. While, far enough from this critical frequency, at 38 Hz rotating speed, a ratio between the major axis and the minor axis of around 2:1 is observed [14]. Then, the shaft orbit could be used for identifying rotor malfunctioning, which is of great significance in diagnosis of rotordynamics machinery. It

can be highlight from this research that rotor orbit could be an important data source for the operation prognosis of the rotating machinery.

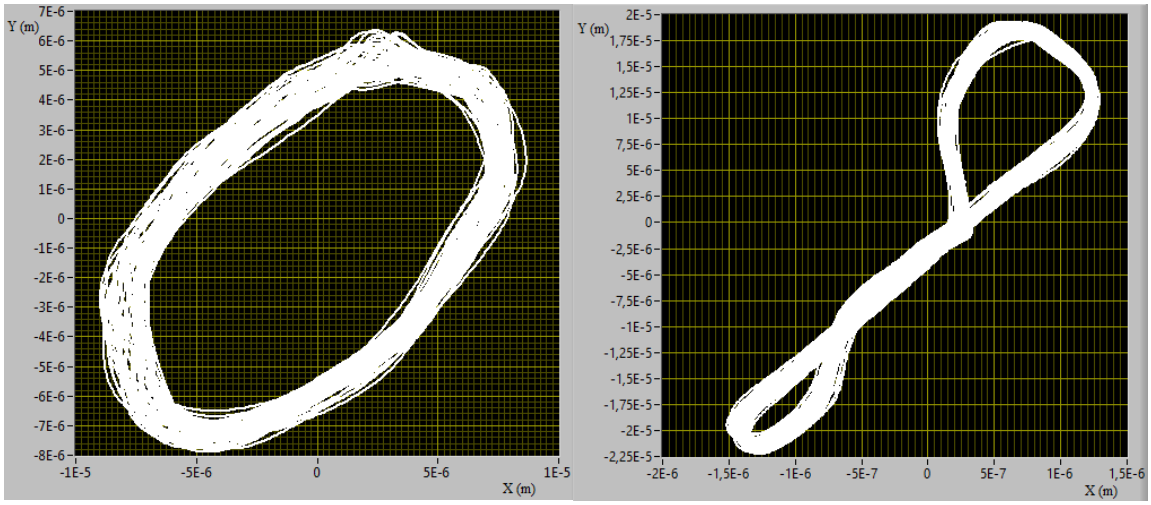

a) b)

Figure 11. Multi-stage rotor orbit X/Y at a rotating speed of, a) 38 Hz and b) 48 Hz.

The model solved in Matlab has been executed with rotation around the z axis operating at 0 – 6000 rpm. The results for the seven-stage rotor are presented in the Campbell diagram, as the Figure 12 shows. The Campbell diagram shows the way the natural frequencies of the rotor vary with respect to the speed of operation owing to the gyroscopic moments.

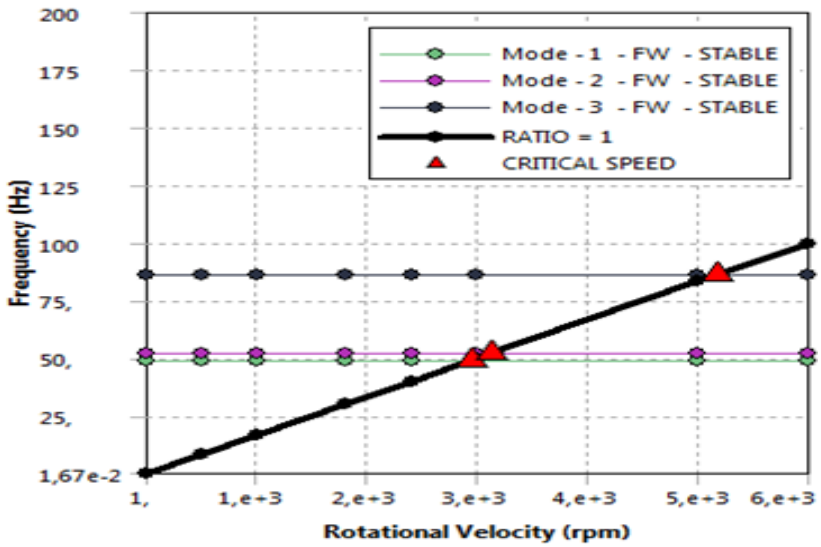

Figure 12. Campbell diagram for the multi-stage rotor.

The results obtained for the first critical speed are presented in Table 3, where the values found by the numerical model and the experimental measurement are compared. The first lateral critical speed obtained from the numerical model of finite elements solved in Matlab

is presented at 2976.1 rpm, while in the Ansys solution it is presented at 2951.7 rpm. The percentages of variation with respect to the values obtained in the experimental measurement are 3.3% and 2.5% respectively.

Table 3. Results for the first lateral critical speed of the multi-stage rotor.

Method	First lateral critical speed [rpm]	% Error*
Current model	2976.1	3.3
Ansys	2951.7	2.5
Experimental measurement	2880	-

* with respect to the experimental value.

At 98 Hz (5880 rpm), the second lateral critical speed is verified experimentally, identified by an increase of ~3.4 times the amplitude of lateral vibration severity with respect to its nominal operation conditions. The results for the second critical speed are presented in Table 4. It is presumed that the increase of the error in the prediction of the second critical speed, both in the proposed model and in the finite element model, is due to variations in the stiffness and damping parameters of the supports that the theoretical models do not contemplate. This can be caused, for example, by the variation in the temperature of the bearings and the lubricant.

Table 4. Results for the second lateral critical speed of the multi-stage rotor.

Method	Second lateral critical speed [rpm]	% Error*
Current model	6453.6	9.8
Ansys	5172.8	-12.0
Experimental measurement	5880	-

*with respect to the experimental value.

The modal forms that the rotor adopts when passing through the critical lateral speeds are presented in Figure 13.

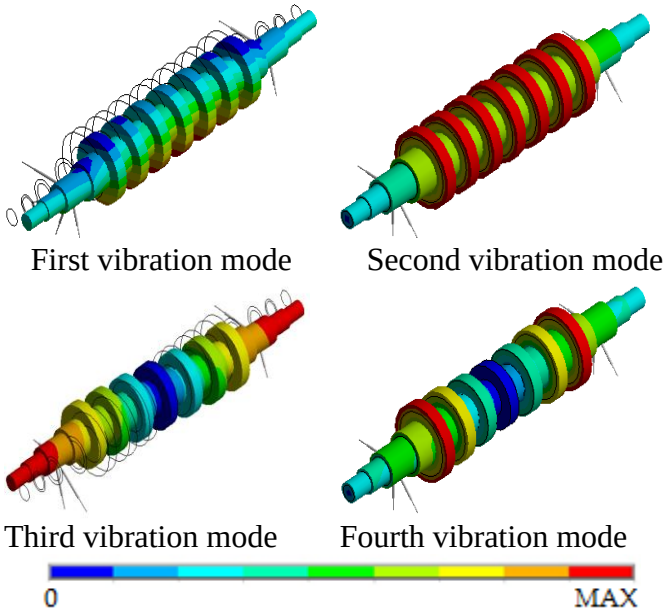

Figure 13. Modal forms for the multi-stage rotor.

The first two vibration modes have a semi-rigid elliptical behavior, while the third and fourth modes have a semi-rigid conical behavior owing to the anisotropy properties in the bearings.

Table 5 shows the results for the rotor subjected to a 2 g unbalance mass located in the angular phase at zero degrees. The unbalance is placed consecutively on each of the rotor impellers.

Table 5. Results for the first lateral critical speed of the multi-stage rotor.

Impeller where the unbalance is located	First lateral critical speed [rpm]		% Error*
	Current model	Experimental measurement	
1	1616.2	1500.1	7.7 %
2	1604.0	1500.1	6.9 %
3	1587.3	1500.1	5.8 %
4	1630.6	1500.1	8.7 %
5	1545.9	1500.1	3.1 %
6	1623.9	1500.1	8.2 %
7	1620.6	1500.1	8.0 %

* with respect to the experimental value.

The maximum error found for the multi-stage rotor current model solved in Matlab, and considering unbalance effects, is 8.7% with respect to the experimental value. The above is attributed to the considerations taken when establishing the data collection frequencies in the experimental measurement.

When changing the angular phase of the mass to induce unbalance in the rotor, the results of the mathematical model and the experimental analysis do not show considerable changes with respect to those presented in the previous table.

CONCLUSIONS

The theoretical model developed meets expectations owing to its level of accuracy and prediction of lateral vibration behavior in the seven-stage rotor. The results of the mathematical model for the determination of the first two lateral critical speeds differ in 3.3% and 9.8%, with respect to the experimental results.

The theoretical and experimental determination of the vibration modes and the critical speeds confirm that, for the nominal operation of the multi-stage rotor, the rotor must necessarily pass through the first critical speed at 48 Hz, where an increase of 1.4 times in the amplitude of the vibration severity is recorded. Besides, the second critical speed is presented at 98 Hz and shows an increase of 3.4 times in the amplitude levels of vibration severity with respect to the values obtained in the nominal frequency of rotor operation.

When the rotor is balanced, the first critical speed is presented at 48 Hz (2880 rpm). When adding an unbalance mass of 2 g in any of the impellers, this speed is presented at 25 Hz (1500.1 rpm). Based on this, we conclude that the effect of the unbalance induced in the rotor by addition of mass causes the frequencies, where critical speeds are normally presented when the rotor is properly balanced, to move to lower frequencies. The theoretical model of the multi-stage rotor solved in Matlab and considering the effects of unbalance, presents a percentage variation of up to 8.7% with respect to the experimental value. This variation is attributed to the considerations taken when establishing the data collection frequencies in the experimental measurement and the residual unbalance of the multi-stage rotor.

The importance of the theoretical model presented in this paper is that despite including the elastic and damping properties of the rotor and supports, gyroscopic effects and unbalance of the impellers, maintains a high level of simplicity. This leads to a low computational cost, but keeping the error below 10%, even for cases of unbalance. The current model must be used with care in the analysis of critical speeds in turbo machinery. It is recommended only for cases of small unbalances and considering a probable region of critical speed consisting of a bilateral band of ± 10% around the calculated critical speeds.

ACKNOWLEDGMENT

The authors would like to thank the research office at the Universidad Nacional de Colombia and the Universidad de Ibagué for their support received for the development of this research.

REFERENCES

[1] Rieger NF. The scientific work of jorgen lund and a personal assessment of its significance. Journal of Vibration and Acoustics. 2003; 125: 441-444.

[2] Reyes D. Harmonic analysis of a non-symmetric rotor including gyroscopic effect with MEF. Memories of XVIII Annal International SOMIM Congress Mexico, Mexico. 2010.

[3] Yao J, Liu L, Yang F, Scarpa F, Gao J. Identification and optimization of unbalance parameters in rotor-bearing systems. Journal of Sound and Vibration. 2018; 431: 54-69.

[4] Genta G. Dynamics of rotating systems. Chapter 15. Three-Dimensional Modeling of Rotors based on FEM. Torino Italy: Published by Springer. 2009.

[5] Wang S, Wang Y, Zi Y, Li B, He Z. Reduced-order modeling for rotating rotor-bearing systems with cracked impellers using three-dimensional finite element models. Journal of Sound and Vibration. 2015; 355: 305-321.

[6] Chen Y, Wang J, Guo Z. Critical Speed and Unbalance Response of the Locomotive Motor Rotor. Recent Patents on Mechanical Engineering. 2016; 9(2): 168-176.

[7] Wang S, Zi Y, Wang Y, He Z. A 3D nonlinear finite element method for the dynamic analysis of rotating rotor with a transverse crack. Science China Technological Sciences. 2017; 60(2): 219-231.

[8] Behera SK, Parhi DR, Das HC. Application of genetic algorithm for crack diagnosis of a free-free aluminum beam with transverse crack subjected to axial and bending load. Journal of Mechanical Engineering and Sciences. 2018; 12(3): 3825-3851.

[9] Yang Y, Wang J, Wang X, Dai Y. A general method to predict unbalance responses of geared rotor systems. Journal of Sound and Vibration. 2016; 381: 246-263.

[10] Green R. Gyroscopic effects of the critical speeds of flexible rotors. Journal Applied Mechanics. 1948; 15(4): 369-376.

[11] Yamada H, Taura H, Kaneko S. Numerical and experimental analyses of the dynamic characteristics of journal bearings with square dimples. Journal of Tribology. 2018; 140(1): 011703.

[12] ISO. International organization for standardization. Mechanical Vibration - Evaluation of machine vibration by measurements on non-rotating. Technical Paper: 10816; 1998.

[13] Mendivelso C. Modeling and analysis of the rotor dynamics behavior of an asymmetric axis subjected to combined lateral and torsional loads. Master's Thesis in Mechanical Engineering, Universidad Nacional de Colombia. 2014.

[14] Karimkhany M, Ranjbar M, Amirinejhad MK. Effects of Impeller Gap on Rotor Vibration in a High Speed Centrifugal Compressor: A Numerical and Experimental Analysis. International Journal of Engineering. 2017; 30(5): 814-820.